Journal of Molecular Medicine (2026) 104:23
https://doi.org/10.1007/s00109-025-02625-x

ORIGINAL ARTICLE

2,8-Dihydroxyadenine disrupts epithelial integrity and alters kidney cell phenotype in vitro

Hildur Run Helgudottir[1] · Runolfur Palsson[1,2] · Vidar Orn Edvardsson[1,3] · Thorarinn Gudjonsson[1,4]

Received: 6 May 2025 / Revised: 14 October 2025 / Accepted: 19 October 2025
© The Author(s) 2026

Abstract

Adenine phosphoribosyltransferase (APRT) deficiency is an autosomal recessive disorder that causes accumulation of 2,8-dihydroxyadenine (DHA) in the urinary tract, leading to kidney stones and chronic kidney disease (CKD). Progression to end-stage kidney disease can occur without timely treatment. The xanthine oxidoreductase inhibitors, allopurinol and febuxostat, block DHA generation and halt or delay stone formation and CKD progression. Some patients do not tolerate xanthine oxidoreductase inhibitor treatment, necessitating new therapeutic approaches. This study aimed to investigate how DHA influences structural and molecular changes in HK-2, HEK293, and MDCK kidney cells. DHA exposure reduced cell viability and impaired migration in all cell lines. Increased expression of the adhesion protein CD44 was observed adjacent to DHA crystals in HEK293 and HK-2 cells. Transepithelial electrical resistance measurements in MDCK cells indicated reduced epithelial integrity following DHA exposure. RNA sequencing of DHA-treated HK-2 cells revealed gene expression changes, with upregulation of TNF-α and mTORC1 signaling and downregulation of epithelial to mesenchymal transition and oxidative phosphorylation. Functional enrichment analysis highlighted pathways related to cell cycle regulation, inflammation, and metabolic processes. These findings show that dose-dependent DHA toxicity interrupts cell migration and epithelial integrity. CD44 may contribute to crystal adhesion, and thus, represents a potential therapeutic target in DHA crystal nephropathy.

Key messages

- DHA reduces kidney cell viability and migration in a dose-dependent manner.
- DHA disrupts epithelial integrity in MDCK cells, lowering TEER values.
- CD44 expression increases adjacent to DHA crystals with increased DHA concentration.
- RNA sequencing shows that DHA upregulates TNF-α, mTORC1, and stress pathways.
- DHA alters gene expression, affecting inflammation, metabolism, and EMT.

Keywords APRT deficiency · CD44 · RNA sequencing · Cell viability · Epithelial barrier integrity

Introduction

Adenine phosphoribosyltransferase (APRT) deficiency (OMIM102600) is a rare autosomal recessive disorder of adenine metabolism that results in the urinary excretion of large amounts of the poorly soluble When dividing 2,8-dihydroxy-adenine (DHA) between lines use: 2,8-dihydroxy- adenine (DHA) causing urinary tract stone formation, crystal nephropathy, and progressive chronic kidney disease (CKD) [1–3]. The xanthine oxidoreductase (XOR) inhibitors, allopurinol and/or febuxostat, are readily available treatment options that effectively prevent stone formation and CKD progression in patients with APRT deficiency by blocking the conversion

✉ Hildur Run Helgudottir
hrh@hi.is

Thorarinn Gudjonsson
tgudjons@hi.is

1 Faculty of Medicine, School of Health Sciences, University of Iceland, Reykjavik, Iceland

2 Section of Nephrology, Landspitali University Hospital, Reykjavik, Iceland

3 Children's Medical Center, Landspitali University Hospital, Reykjavik, Iceland

4 Section of Laboratory Hematology, Landspitali University Hospital, Reykjavik, Iceland

Published online: 06 January 2026

of adenine to DHA [1–3]. Unfortunately, some affected individuals tolerate neither allopurinol nor febuxostat and, therefore, alternative treatment options are needed.

Traditionally, DHA crystal deposition in the kidneys has been assumed to cause direct mechanical tubular obstruction and nephron destruction, resulting in progressive CKD [2]. Recent studies, however, suggest that inflammatory processes may mediate human crystal-induced kidney injury [4–6]. Although the exact inflammatory mechanisms involved in DHA crystal nephropathy remain unclear, certain mediators such as TNFR1, TNFR2, and CD44 appear to be crucial mediators in animal models of the disorder [7].

Oxalate is a well-studied mediator of human crystal nephropathy in patients with primary hyperoxaluria [8]. Cell culture studies exposing the kidney epithelium to calcium oxalate monohydrate (COM) have found COM crystals to migrate between epithelial cells and adhere to the basement membrane, causing cellular proliferation and affecting tight junction protein polarization and integrity [9, 10]. This is evidenced by diminished transepithelial electrical resistance (TEER) in MDCK cells exposed to COM [9]. CD44, present in kidney epithelial cells, has been found to mediate COM crystal adhesion by facilitating crystal attachment to the tubular epithelium [11, 12]. This adhesion is crucial for crystal binding and kidney stone formation, allowing crystals to anchor and grow instead of being excreted in the urine. Koul et al. conducted a cDNA microarray study on HK-2 cells after exposure to oxalate and explored underlying molecular mechanisms [13]. Within 24 h of oxalate exposure, 750 genes were upregulated and 2276 genes downregulated, with significant changes observed in genes associated with PI3 kinase and MAP kinase pathways [13]. Previous research focusing on the overexpression of the PPM1K gene in HK-2 cells in response to treatment with COM crystals identified 796 differentially expressed genes through RNA sequencing analysis [14].

No studies are available describing the effects of DHA exposure on kidney epithelial cells in vitro. The aims of the current work were to investigate the effects of DHA exposure on cultured kidney cells in vitro, looking for various markers and mediators of injury that could serve as potential therapeutic targets.

Materials and methods

Cell culture

HK-2 cells (CRL-2190), HEK293 cells (CRL-1573), and MDCK cells (CCL-34) were purchased from the American Type Culture Collection (ATCC, Manassas, VA, USA) and cultured in Minimal Essential Medium (MEM) (Gibco; Thermo Fisher Scientific, Waltham, MA, USA) containing 10% fetal bovine serum (FBS) (Invitrogen; Thermo Fisher Scientific, Waltham, MA, USA), 5 mM sodium pyruvate (Gibco; Thermo Fisher Scientific, Waltham, MA), and 1% penicillin/streptomycin (Gibco; Thermo Fisher Scientific, Waltham, MA, USA) at 37 °C with 5% CO_2. DHA was synthesized at the Department of Chemistry, Faculty of Physical School of Engineering and Natural Sciences, University of Iceland. DHA was suspended in cell culture media and diluted to the final concentrations of 60, 120, 240, and 480 µg/mL, which are comparable to those previously found in the urine of patients with APRT deficiency.

Immunocytochemistry

Cells were grown on 8-well removable chamber slides (Ibidi, Gräfelfing, Germany), 8-well µ-slides (Ibidi, Gräfelfing, Germany) and Clipmax 10 cm^2 chamber slide (TPP, Trasadingen, Switzerland). DHA was added to the culture medium in the concentrations of 120 and 480 µg/mL and incubated for 72 h. Control wells contained culture medium only. Antibodies used for immunocytochemistry studies were APRT (21,405–1-AP, Proteintech, Manchester, UK), XOR (55,156–1-AP, Proteintech, Manchester, UK) and CD44 (60224–1-Ig, Proteintech, Manchester, UK). Antibodies bound to target proteins were identified by fluorescein-labeled secondary antibodies (Alexa Fluor, Thermo Fisher Scientific, Waltham, MA, USA) and 4′,6-diamidino-2-phenylindole (DAPI) (Sigma-Aldrich, St. Louis, MO, USA). For staining liquid–liquid interface (LLI) cultures, cells were fixed in 4% paraformaldehyde solution (PFA) in phosphate-buffered saline (PBS). Cells were then fluorescently labeled with 4′,6-diamidino-2-phenylindole (DAPI) and phalloidin (Alexa Fluor, Thermo Fisher Scientific, Waltham, MA, USA). For quantification, individual cells were manually outlined as regions of interest (ROIs) in Fiji (ImageJ). Within each ROI, stress fibers were detected using the ridge detection plugin and per-cell values for total fiber length, mean fiber length, mean fiber width, and fiber count were extracted. Cell-level values were averaged per image to obtain replicate-level data for statistical analysis. Images were acquired using an Olympus FV1200 and Olympus FV4000 confocal microscope (Olympus Corporation, Tokyo, Japan).

Western blotting

Protein was isolated from cells lysed with radioimmunoprecipitation assay (RIPA) buffer containing protease and phosphatase inhibitors (Halt Protease Inhibitor Cocktail, Thermo Fisher Scientific, Waltham, MA, USA). Bradford reagent (BioRad, Hercules, CA, USA) was used to determine protein concentration. Western blot was performed on 4–12% NuPage Bis–Tris gels (Invitrogen, Thermo Fisher Scientific, Waltham, MA) in NuPage MES running buffer

(Thermo Fisher Scientific, Waltham, MA, USA). Protein was transferred from the gel to Immobilon-FL PVDF membrane (Merck-Millipore, Darmstadt, Germany) with NuPage transfer buffer (Thermo Fisher Scientific, Waltham, MA, USA). Membranes were blocked with 5% milk in TBS and incubated overnight at 4 °C with primary antibodies. The following primary antibodies were used for protein detection: anti-APRT (21,405–1-AP, Proteintech, Manchester, UK) 1:1000 and anti-XOR (55,156–1-AP, Proteintech, Manchester, UK) 1:500 with actin (66,009–1-Ig, Proteintech, Manchester, UK) as an endogenous control. Secondary antibodies used were from rabbit or mouse (Li-Cor, Lincoln, MA, USA), and imaging was performed using the Odyssey Infrared Imaging System (Li-Cor, Lincoln, MA, USA).

Cell viability assay

Cell viability was assessed using PrestoBlue™ Cell Viability Reagent (Thermo Fisher Scientific, Waltham, MA, USA). HEK293, MDCK and HK-2 cells were seeded and grown overnight in 10% MEM in a 96-well plate at the density of 1.0×10^4 cells/cm^2, 0.5×10^3 cells/cm^2 and 1.0×10^4 cells/cm^2. DHA was added to the culture medium in the concentrations of 60, 120, 240, and 480 µg/mL and incubated for 72 h. Control wells contained culture medium only. PrestoBlue was added (1/10th of the total volume) to each well and incubated for 2 h, and the absorbance was read on a plate reader at 570 nm and 595 nm.

Wound healing assay

HEK293, MDCK and HK-2 cells were seeded overnight in a 96-well plate at the density of 3.0×10^4 cells/cm^2, 1.25×10^4 cells/cm^2, and 1.75×10^4 cells/cm^2, respectively, to form a semi-confluent monolayer. DHA was then added to the medium in the concentrations of 120 and 480 µg/mL and cultured for 24 h. A straight scratch was made in the monolayer using a sterile 200-µL pipette tip. The wells were washed with PBS to remove debris, and a fresh medium was added to the cells. The plate was then placed in the Incucyte S3 Live-Cell Analysis System (Sartorius, Göttingen, Germany), and phase-contrast photomicrographs were acquired every 2 h. Scratch width was measured at multiple points using the Incucyte S3 software. The average scratch width was calculated at each time point. Data were normalized to the initial scratch width, and migration was expressed as the percentage of wound closure.

Liquid–liquid interface (LLI) transwell cultures

TEER measurements were used to evaluate the integrity of tight junctions in the epithelial cell monolayers. MDCK cells were seeded (7.0×10^5 cells/cm^2) on Transwell filter inserts (Corning 0.4 µm polyester membrane, Corning, NY, USA) and grown until they formed a confluent monolayer. Urine was collected from healthy individuals, sterile filtered through a 0.45-µm mesh and subsequently frozen at −20 °C. Before the experiment, the urine was warmed up to 37 °C and spiked with DHA in the concentrations of 120 and 480 µg/mL. An epithelial volt-ohmmeter (Millicell ERS-2, MilliporeSigma, Burlington, MA, USA) with chopstick electrodes was used to measure resistance across the cell layer every 2–3 days.

RNA isolation and real-time qPCR

Cells were grown in monolayer, and DHA was added to the culture medium in the concentrations of 120 and 480 µg/mL, after which the cells were incubated for 72 h. Control wells contained culture medium only. RNA was isolated using Tri-Reagent (AM9738, Ambion, Thermo Fisher, Waltham, MA, USA) and 1 µg of each RNA sample was reverse transcribed using the LunaScript RT SuperMix Kit (New England BioLabs, Ipswich, MA, USA). Quantitative real-time PCR was performed using SYBR Green Luna Universal qPCR Master Mix (New England BioLabs, Ipswich, MA, USA) as per manufacturer recommendation. Relative expression was determined via calculation of 2-ΔΔCt using the ABI 7500 instrument (Applied Biosystems, Foster City, CA, USA), with GAPDH as the endogenous control for gene expression. Primers were purchased from Integrated DNA Technologies (Coralville, IA, USA) using ready-made human primer pools for HEK293 and HK-2: GAPDH (Hs.PT.39a22214836) and CD44 (Hs.PT.58.3636696). Primers were designed for MDCK: GAPDH (forward: 5′TTCCACGGCACAGTCAAG, reverse: 5′ACTCAGCACCAGCATCAC 3′), CD44 (forward: 5′CCG AGGACCAAGACAGTTCC, reverse: 5′GAGTCGTGGTCT TTGGTAATGG 3′). GAPDH was used as the endogenous control.

RNA sequencing

HK-2 cells in monolayer were treated for 72 h with DHA at 60, 120, and 240 µg/mL, and then RNA was isolated employing TRI-Reagent (Ambion, Thermo Fisher, Waltham, MA, USA). The RNA samples were shipped to BGI Genomics (Shenzhen, Guangdong, China) for RNA sequencing. The expression of RNA transcripts was quantified with Kallisto version 0.50.0 using the Ensembl *human* GRCh38.p14. Gene expression estimates were computed with the sleuth R package v0.30 [15]. Gene set enrichment analysis was performed using the GSEA software v4.3.3 [16]. Pre-ranked gene lists were prepared by ranking the genes (one transcript per gene) according to the significance of differential expression, defined as the q-value times the sign of the log-fold

change and tested for enrichment in the hallmark gene set collection from MSigDB [17].

Statistical analysis

Experiments were carried out in triplicate. Graphs were generated using the GraphPad Prism software v.10.4.2 (GraphPad Software Inc, San Diego, CA). One-way analysis of variance (ANOVA) using Dunnett's multiple comparison test or unpaired t tests was employed to determine statistical significance. *P*-values below 0.05 were considered significant ($*p \leq 0.05$, $**p \leq 0.01$, $***p \leq 0.001$, $****p \leq 0.0001$). For viability testing, significance was based on *p*-values below 0.05 ($*p < 0.05$). To ensure the accuracy of the dataset, outliers were identified by using Grubbs' Test for outliers and removed in GraphPad Prism.

Results

APRT and XOR expression in kidney cell lines

In this study, we used HEK293, MDCK and HK-2 kidney cell lines, representing a wide range of phenotypic heterogeneity. MDCK cells were isolated from the distal tubules of cocker spaniel [18], HK-2 was isolated from the proximal tubule of a healthy human kidney [19], and HEK293 are fetal kidney cells, isolated from an aborted fetus [20]; thus, these 3 cell lines were considered to be a good representative model for studying inflammation and fibrosis in the kidney in APRT deficiency. Immunofluorescence staining revealed distinct localization patterns of APRT and XOR across the cell lines (Fig. 1a). APRT (red staining) exhibited strong cytoplasmic and nuclear staining in HEK293 cells but showed weaker or nearly absent staining in HK-2 and MDCK cells. By contrast, XOR (green staining) was detected in all three cell lines, showing a diffuse cytoplasmic localization. Nuclei were counterstained with DAPI (blue staining) to confirm cell morphology and distribution. The specificity of APRT and XOR immunostainings was confirmed by secondary antibody-only negative controls, which showed no signal (Fig. S1). To further validate expression, qPCR demonstrated that APRT mRNA levels were highest in HEK293 cells and lower in HK-2 and MDCK cells, consistent with the immunofluorescence pattern (Fig. S1). Western blotting confirmed protein expression of both APRT and XOR across all cell lines (Fig. 1b).

Decreased viability and migration of kidney cell lines after DHA exposure

The cell lines used in this study were exposed to different DHA concentrations, similar to those previously observed in the urine of APRT deficiency patients [21]. After 72 h of incubation with DHA at the concentration of 60, 120, 240, and 480 µg/mL, decreased viability was observed in a dose-dependent manner. The greatest decrease in viability, to approximately 40%, was observed in HEK293 cells at the highest DHA concentration, (Fig. 2a). The viability of MDCK cells and HK-2 cells also decreased, but to a lesser degree; the viability of MDCK and HK-2 cells were 80 and 70% after 72 h, respectively at the highest DHA concentration (Fig. 2a).

Wound closure was evaluated using a scratch assay after treatment with DHA for 24 h at two different concentrations, 120 and 480 µg/mL. MDCK cells showed slower wound closure following the addition of DHA and did not close the wound within 24 h when compared with controls (Fig. 2b). The HEK293 control cells achieved full closure within 72 h, whereas cells treated with 480 µg/mL DHA closed only ~ 50% of the wound by this time point (Fig. 2b). The HK-2 cells migrated at a slower rate than the other cell lines and were not able to close the wound within 72 h in the control wells. At 72 h, control wells containing HK-2 cells reached ~ 95% closure compared to ~ 80% and ~ 70% for the 120 and 480 µg/mL DHA groups, respectively (Fig. 2b). Phase-contrast microscopy demonstrated decreased cell density and the presence of cellular debris across all cell lines after DHA treatment (Fig. 2c), indicating that reduced viability (Fig. 2a) likely contributed together with impaired migration to the slower wound closure observed.

DHA decreases epithelial integrity in MDCK cells

TEER was measured to determine the strength of the epithelial barrier. MDCK cells formed a polarized layer when cultured on a transwell polyester membrane. The cells were grown in two different on-top cultures, with either media or urine on top, with and without DHA at the concentrations of 120 and 480 µg/mL. COM (100 µg/mL) was used as a positive control because it has previously been shown to decrease TEER [9, 22]. The relative TEER (TEER measurements compared with control) decreased after treatment with DHA at both 120 and 480 µg/mL (Fig. 3a). On day 7, there was a significant drop in TEER for both DHA concentrations in the media-on-top culture, whereas the COM-treated cells did not show a significant decrease in TEER (Fig. 3b). In cultures with urine on top, all DHA concentrations showed a significant decrease in TEER, with the drop being most pronounced in the cells exposed to DHA 120 and 480 µg/mL when compared with COM (Fig. 3b). Filters were stained with phalloidin and DAPI to visualize the cell layers, and a Z-stack image was captured. Phalloidin staining revealed concentration-dependent changes in actin organization, with 480 µg/mL DHA inducing pronounced stress fiber formation

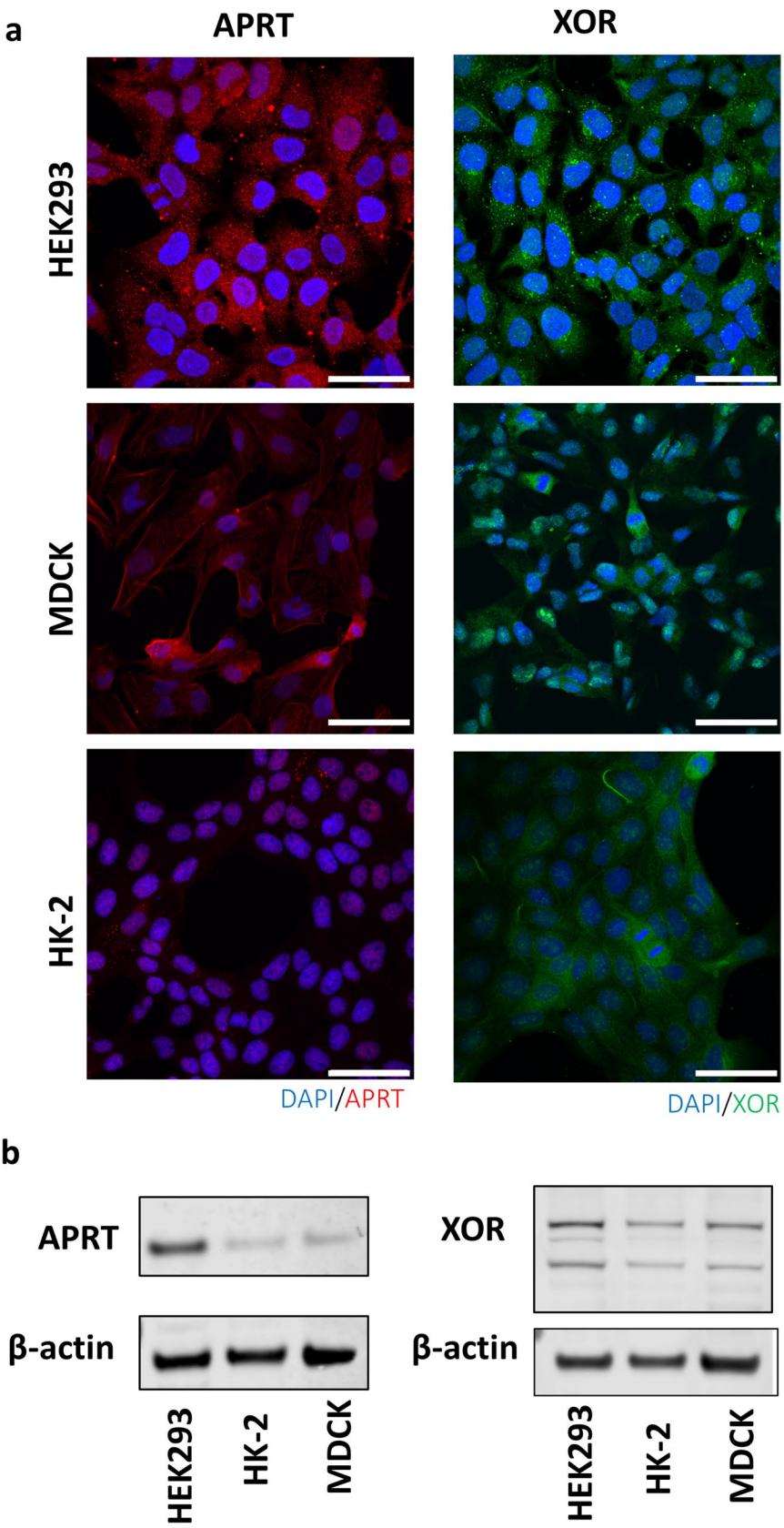
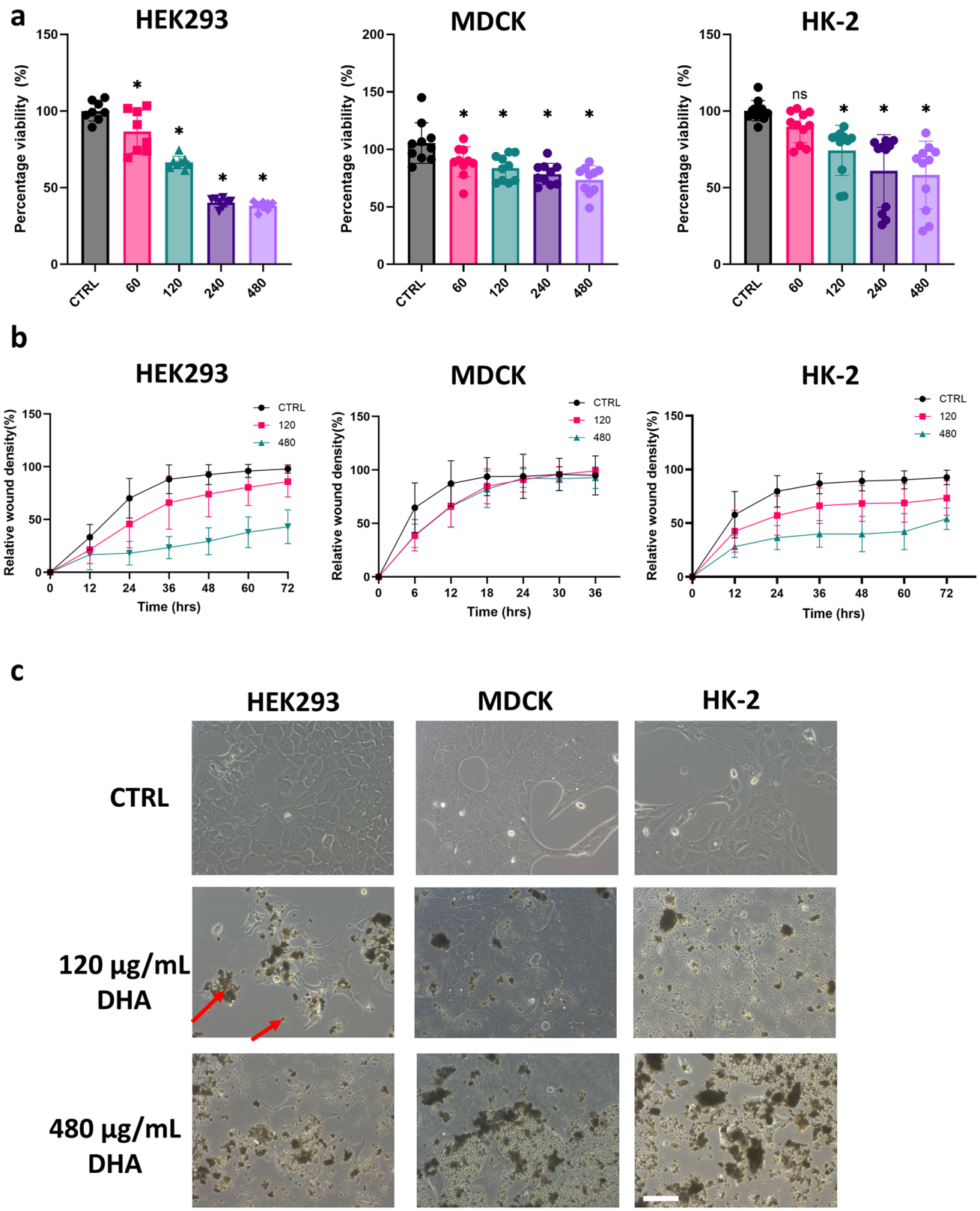


Fig. 1 Adenine phosphoribosyltransferase (APRT) and xanthine oxidoreductase (XOR) expression in kidney cell lines. **a** Representative confocal microscopic images of HEK293, MDCK, and HK-2 cells stained for adenine phosphoribosyltransferase (APRT, red) and xanthine oxidoreductase (XOR, green). **b** Representative Western blots showing APRT and XOR protein expression in HEK293, HK-2, and MDCK cells. GAPDH was used as a loading control. Bands correspond to the expected molecular weights (APRT ~ 18 kDa, XOR ~ 150 kDa). Scale bar, 50 µm



and intermediate changes at 120 µg/mL. COM treatment also altered actin morphology, consistent with reduced epithelial integrity. Quantitative analysis of actin fibers (length, width, and number per cell) confirmed an increase in the number of stress fiber after DHA exposure (Fig. S2).

◂**Fig. 2** 2,8-Dihydroxyadenine (DHA) treatment affects viability and wound closure of kidney cell lines cultured in monolayers. **a**. Viability of HEK293, MDCK and HK-2 cells assessed with and without 2,8-dihydroxyadenine (DHA) at concentrations of 60, 120, 240 and 480 µg/mL for 72 h. All cell lines showed decreased viability following DHA treatment. Error bars represent the standard error of the mean (SEM). **b**. Wound closure was assessed using a scratch assay in HEK293, MDCK, and HK-2 cells with and without 24 h treatment with DHA at concentrations of 120 and 480 µg/ml. All cell lines showed decreased wound closure time in response to DHA. **c**. Phase contrast images of HEK293, MDCK, and HK-2 cells with and without DHA (120 and 480 µg/ml) in monolayer culture. Red arrows indicate the presence of DHA in cell culture media and on the surface of cells. Scale bar: 75 µm

CD44 expression increased with DHA exposure

To examine the crystal-binding phenotype characterized by CD44 expression, the cell lines were treated with two different concentrations of DHA, 120 and 480 µg/mL, for 72 h. RNA sequencing of HK-2 cells demonstrated progressively stronger CD44 gene expression with increasing DHA concentrations (60–240 µg/mL) (Fig. 4a). To validate these findings, we conducted qPCR analysis of HK-2 cells (Fig. 4b). While 120 µg/mL DHA treatment resulted in a modest, non-significant increase in CD44 expression, the exposure to 480 µg/mL DHA induced a statistically significant upregulation ($p < 0.05$). In HEK293 cells, both CD44 gene (Fig. 4b) and protein expression were increased at the higher DHA concentration (Fig. 4c). MDCK cells did not show increased CD44 gene expression; however, CD44 protein expression was elevated adjacent to the DHA crystals when evaluated by both light and confocal microscopy (Fig. 4c). As shown in the negative control (secondary antibodies only), DHA was neither autofluorescent nor bound by the secondary antibodies (Fig. S3).

Dose-dependent upregulation of TNFA and mTORC1 and downregulation of epithelilal-to-mesenchymal transition in HK-2 cells revealed by RNA sequencing

The separation of experimental conditions via principal component analysis (PCA), with clustering based on the DHA concentration (Fig. 5a), reflected condition-specific changes in gene expression, with the greatest separation observed between control and DHA-treated cells. The volcano plots (Fig. 5b-d) illustrate the distribution and magnitude of gene expression changes at increased DHA concentrations. Figure 7a quantifies the progressive increase in the number of significantly differentially expressed genes, demonstrating a concentration-dependent rise in differentially expressed gene counts.

Hallmark gene set enrichment scores, visualized with a heatmap, revealed that increasing DHA concentrations led to upregulation of pathways such as E2F targets, G2M checkpoint, and TNF-α 4signaling, while epithelial-to-mesenchymal transition (EMT) and oxidative phosphorylation were downregulated (Fig. 6a). Positive and negative enrichment plots for specific hallmark pathways highlighted the activation of mechanisms such as mTORC1 and TNF-α signaling, and suppression of processes including DNA repair and EMT in HK-2 cells exposed to high DHA concentration (240 µg/mL) (Fig. 6b and c).

The overlap of upregulated and downregulated genes across the three DHA concentrations is shown in Fig. 7, displaying a Venn diagram of 141 upregulated genes shared across all conditions (Fig. 7a), and the top 10 upregulated expression patterns visualized as a heatmap (Fig. 7b). The top 10 genes were SLC3A2, GFPT1, CRYM, ITGB5, UBE2I, CCND1, SIGLEC15, ARHGAP22, TMEM158, and ANGPTL4. Similarly, 243 overlapping downregulated genes were identified (Fig. 7c), with the top 10 most significantly downregulated genes highlighted in a heatmap (Fig. 7d). These genes were ADRB2, CCDC90B, RPS18, NDUFB3, FOXp1-DT, ATP5PO, RPS7, BRINP1, RPL23A, and OST4. As these gene groups were quite diverse, functional analyses were carried out. Functional enrichment of these gene sets is presented as dot plots displaying enriched GO biological processes for upregulated and downregulated genes (Fig. 7e-f). Pathways such as the ERK1 and ERK2 cascade and positive regulation of angiogenesis are recognizable among upregulated genes, while downregulated genes are associated with cytoplasmic translation, oxidative phosphorylation, and cell migration.

Discussion

In the current study, DHA exposure induced dose-dependent changes in gene and protein expression, cell viability, cell migration, and epithelial integrity in kidney cell lines in vitro. In HK-2 cells, RNA sequencing revealed upregulation of TNF-α and mTORC1 and downregulation of EMT and oxidative phosphorylation, with increasing differential gene expression at higher DHA concentrations. Key upregulated genes included SLC3A2, CCND1, and ANGPTL4, while ADRB2, RPS18, and NDUFB3 were downregulated. Angiopoietin-like 4 (ANGPTL4) is a glycoprotein involved in regulating lipid metabolism, inflammation, and vascular permeability [23]. Recent studies have implicated ANGPTL4 as a significant contributor to kidney fibrosis, particularly in the context of diabetic kidney disease [24]. CD44 expression increased with DHA exposure, with HEK293 cells showing elevated levels of gene and protein expression and MDCK cells exhibiting strong CD44 protein staining adjacent to the DHA crystals. DHA reduced cell viability, particularly of HEK293 cells, and impaired migration of MDCK and HEK293 cells. MDCK cells also showed decreased epithelial integrity, indicated by a significant TEER drop.

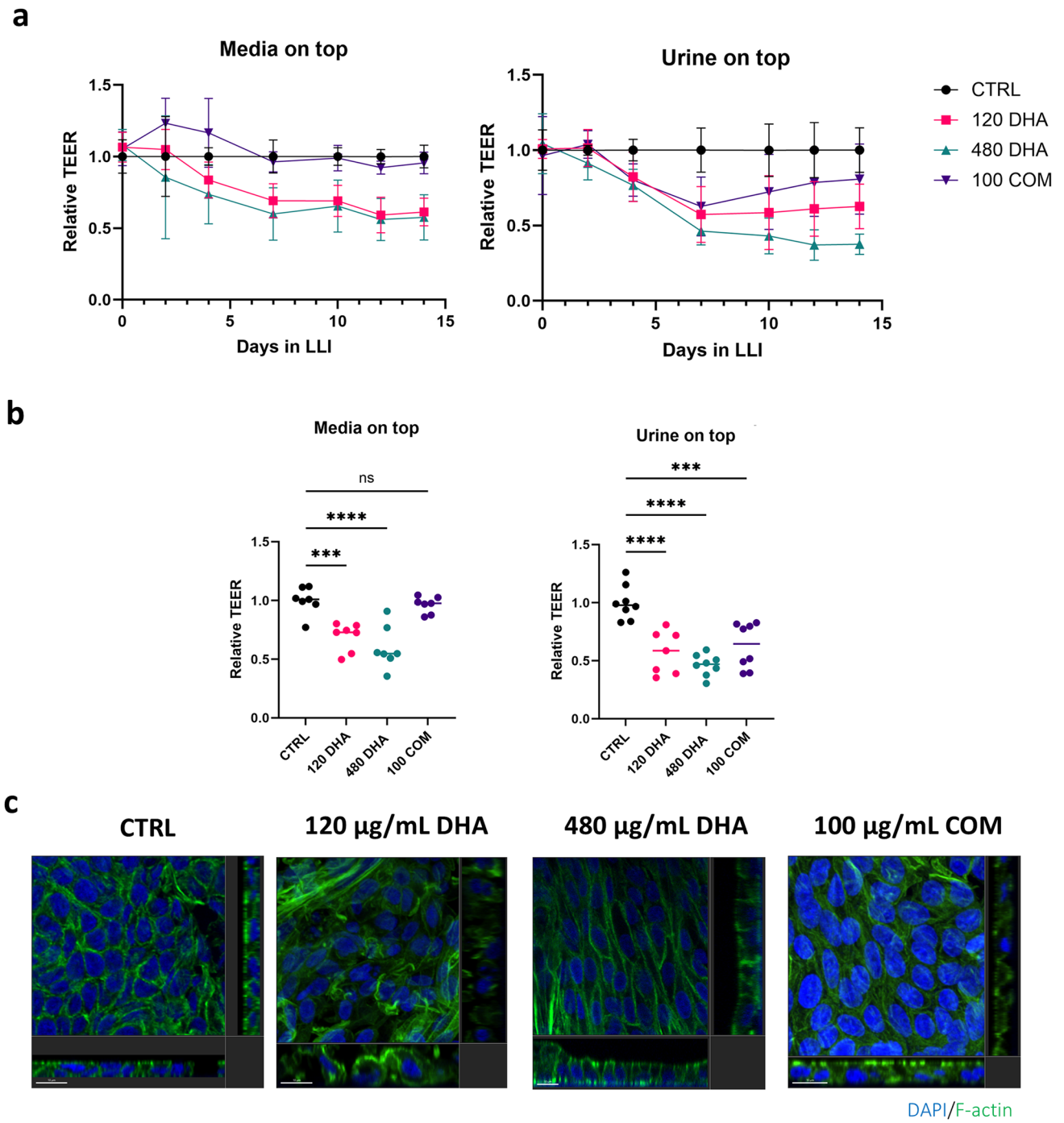


Fig. 3 2,8-Dihydroxyadenine (DHA) reduced transepithelial electrical resistance (TEER) in MDCK cells. MDCK cells were grown on a transwell polyester membrane to form a polarized cell layer. Cultures were treated with and without DHA or calcium oxalate monohydrate (COM) in media or urine. a. Relative TEER, calculated with control wells as baseline, decreased with addition of DHA, both with urine on top and media on top. COM was used as a positive control. b. Relative TEER had significantly decreased on day 7 in the DHA-treated cells. One outlier was removed from the 120 µg/mL DHA group using Grubb's test in GraphPad Prism. Error bars represent the standard error of the mean (SEM). c. The filters were stained with phalloidin (F-actin) and DAPI (nuclei) to confirm the presence of cell layers, and Z-stack imaging performed. Both horizontal and vertical views are shown for the control (CTRL) as well as for cells treated with DHA (120 and 480 µg/mL) or COM (100 µg/ml). Scale bar: 10 µm

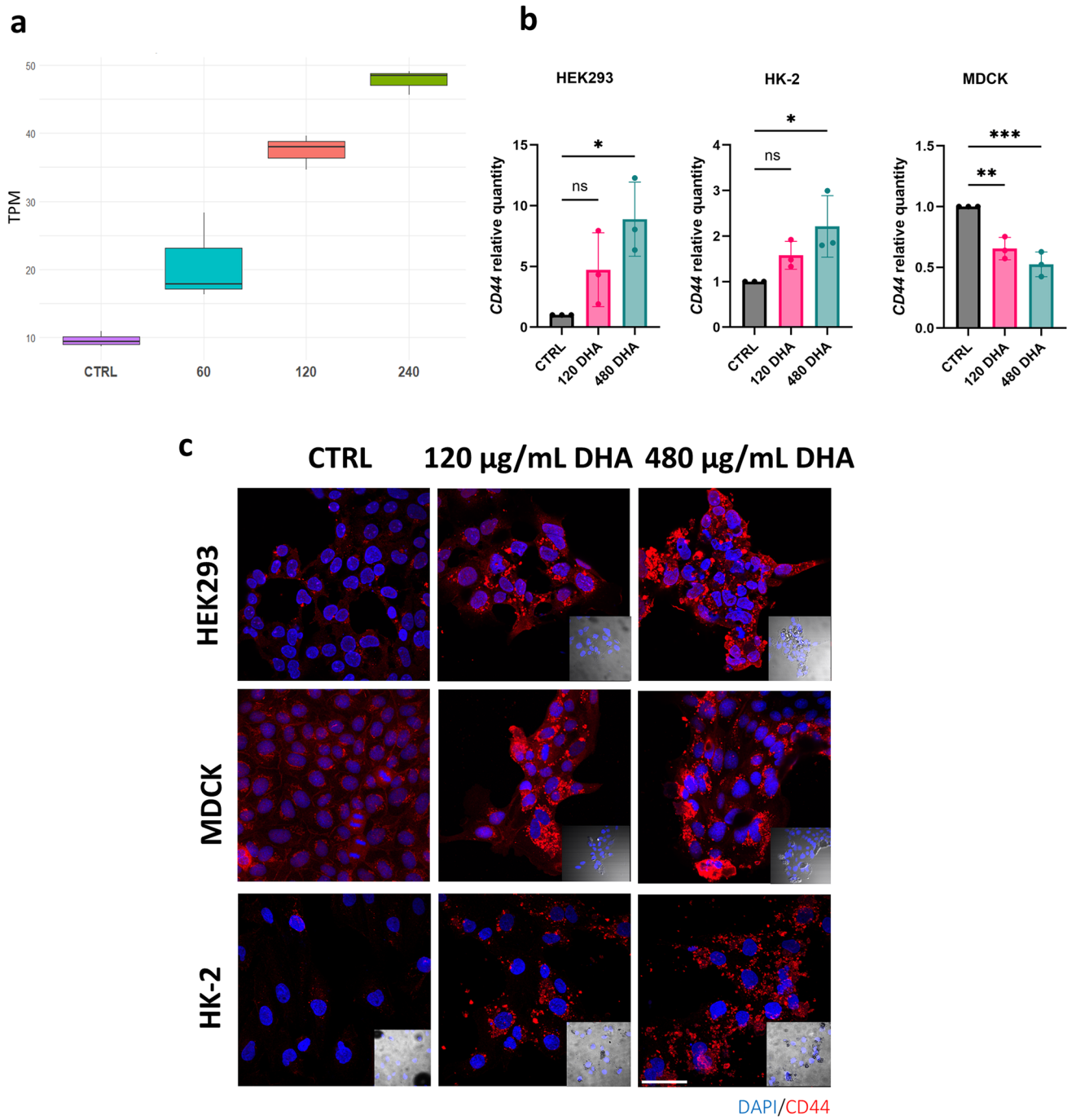


Fig. 4 Upregulation of CD44 expression following 2,8-dihydroxyadenine (DHA) exposure. a. RNA sequencing of HK-2 cells treated with DHA (60–240 µg/mL), showed a dose-dependent increase in CD44 transcript levels expressed as transcripts per million (TPM). b. CD44 was upregulated in HEK293 and HK-2 cells when treated with DHA at 120 and 480 µg/mL for 72 h. MDCK cells did not show upregulation of CD44 gene expression. Error bars represent the standard error of the mean (SEM). c. CD44 protein expression increased in HEK293, MDCK, and HK-2 cells after treatment with DHA at 120 and 480 µg/mL for 72 h. Scale bar: 50 µm

We included APRT and XOR profiling to establish the baseline purine salvage and oxidation capacity of the kidney cell lines used in the study. In the absence of APRT activity, adenine is oxidized by XOR to DHA. The oxidase form of XOR can generate reactive oxygen species, which may amplify cellular injury [25]. Although our model primarily includes exogenous DHA exposure, differences in APRT and XOR expression patterns between cell lines could influence their susceptibility to stress and crystal toxicity. The higher APRT expression observed in HEK293 cells, compared with

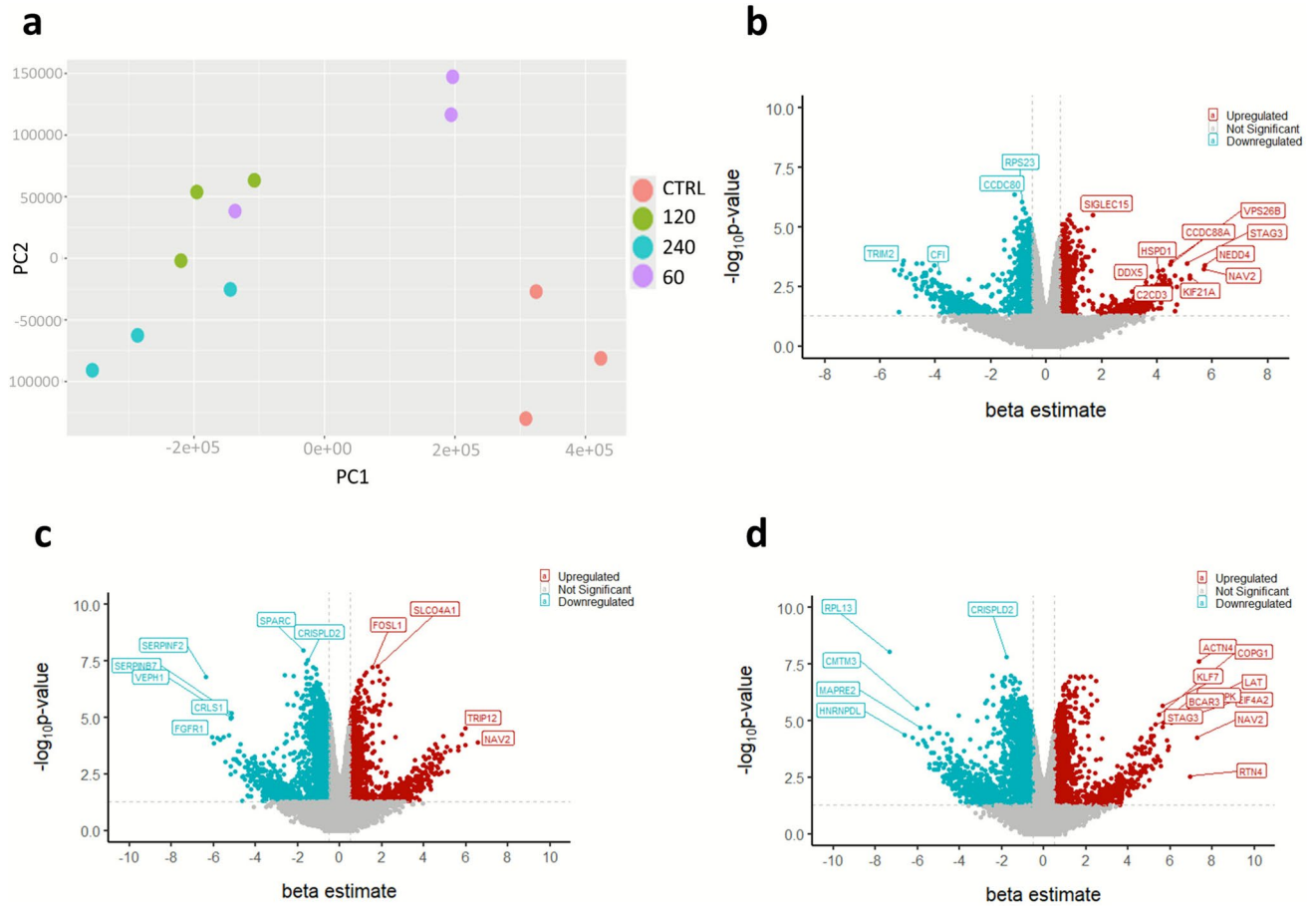
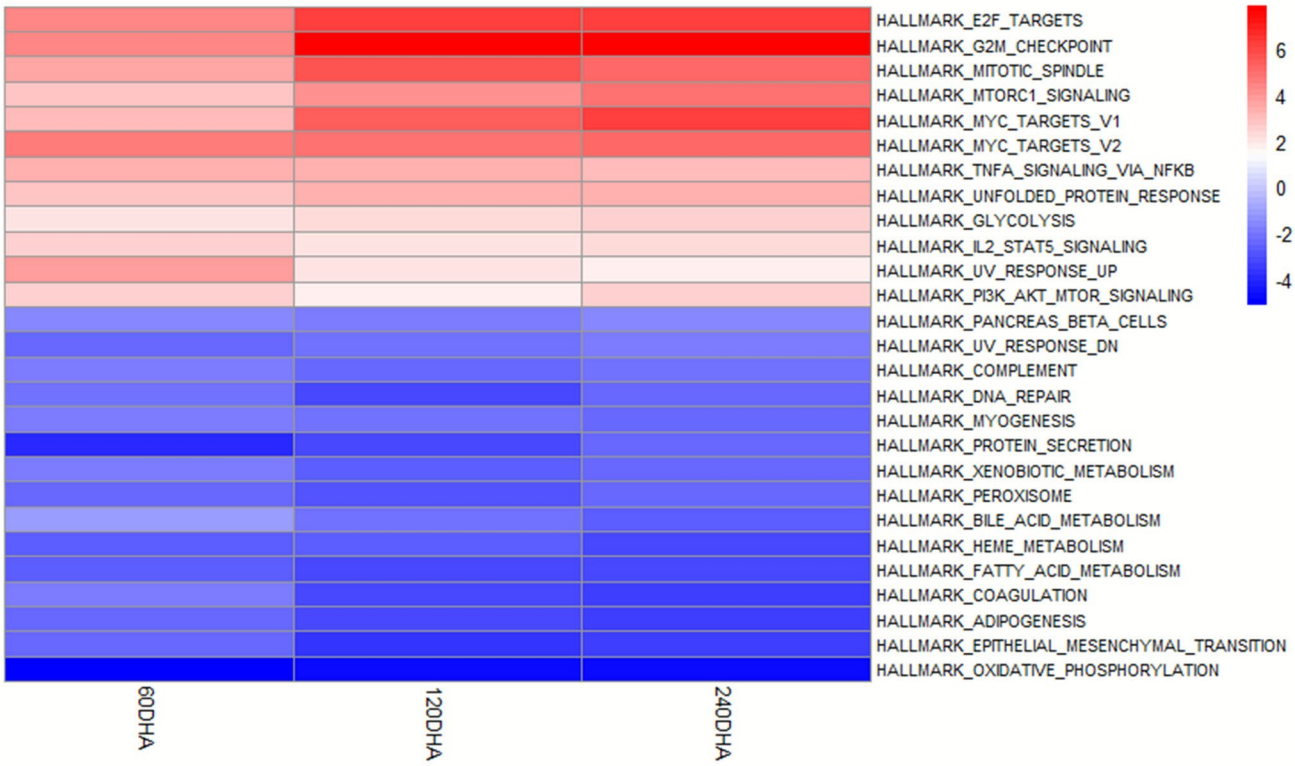


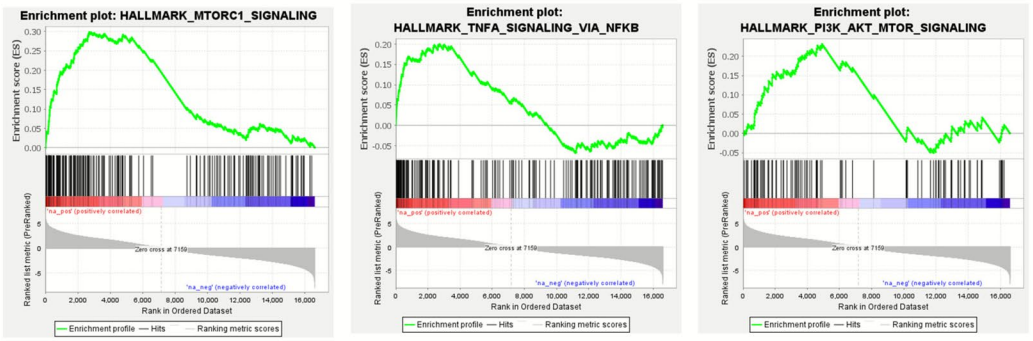
Fig. 5 RNA sequencing results highlight differential gene expression with increasing 2,8-dihydroxyadenine (DHA) concentrations. a. Principal component analysis plot reveals clustering of samples based on RNA expression, showing clear separation according to experimental conditions. b. Volcano plot for HK-2 cells treated with DHA 60 µg/mL versus control shows limited changes, with only a small subset of genes demonstrating high significance. c. Volcano plot for HK-2 cells treated with DHA 120 µg/mL versus control shows significant increase in gene expression compared to DHA 60 µg/mL. d. Volcano plot for HK-2 cells treated with DHA 240 µg/mL versus control displays widespread and highly significant changes in gene expression, reflecting concentration-dependent effects. The overall increase in differentially expressed genes across concentrations is summarized in Fig. 7a

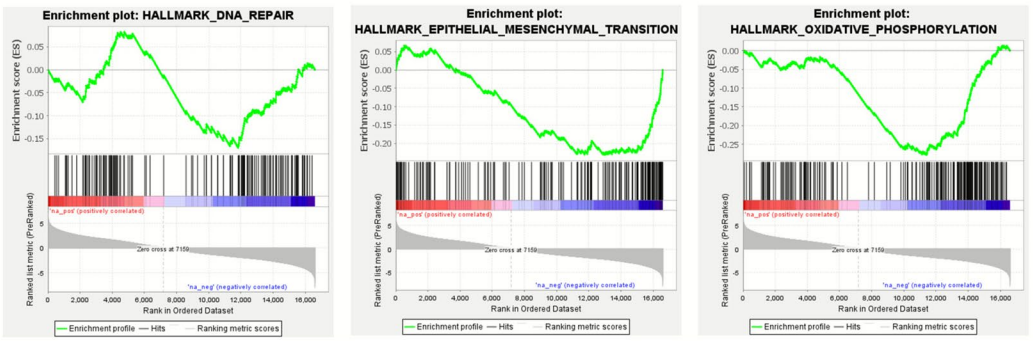
HK-2 and MDCK cells, may partially explain the heterogeneity in cell responses.

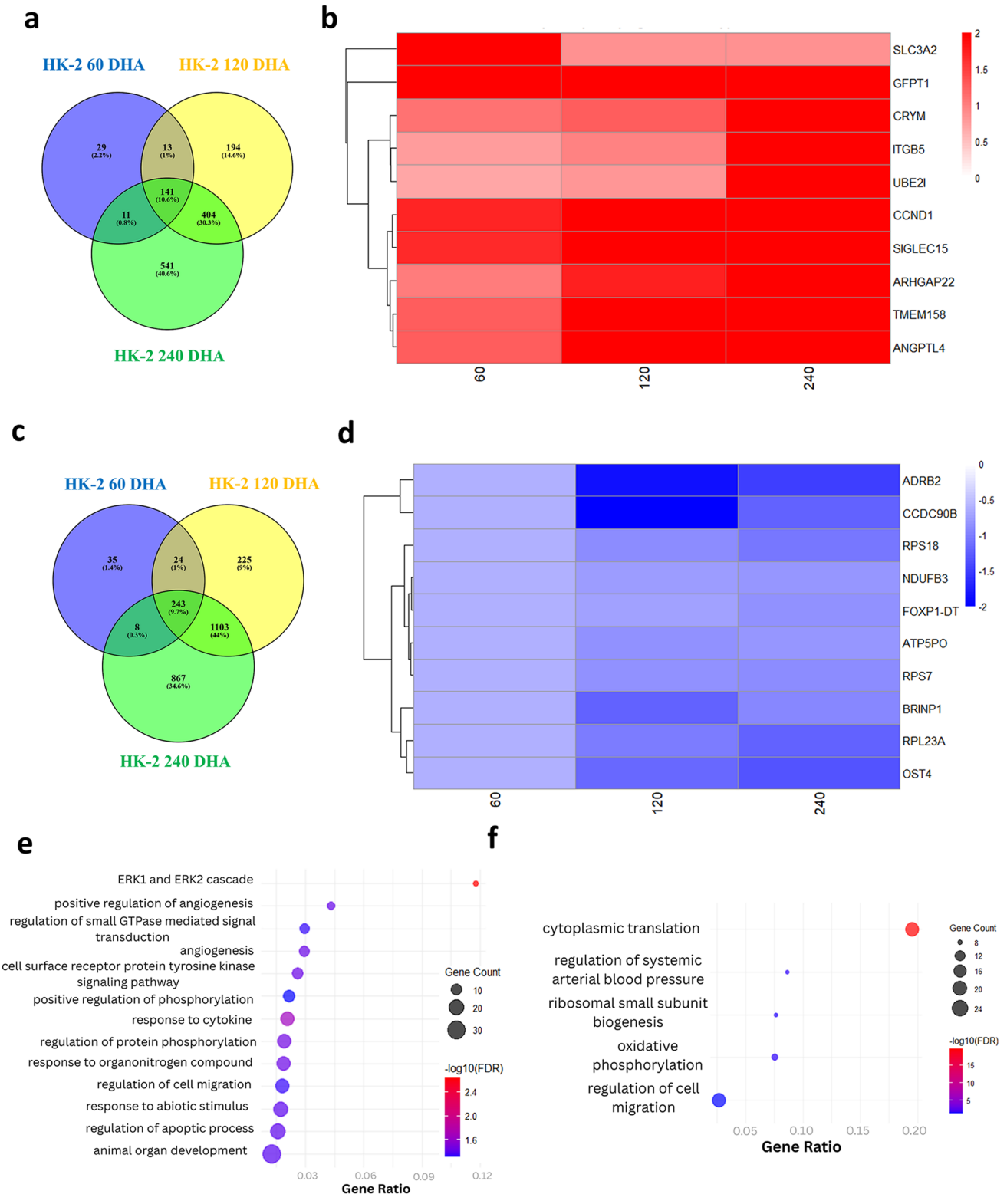
The impaired wound closure following DHA exposure should be interpreted with caution. Scratch assays reflect not only migration but also proliferation and viability. Because DHA reduced viability and induced visible cell debris, reduced wound closure likely reflects a combination of impaired migration and cell death/loss. Future migration-specific assays under non-proliferative conditions will be needed to assess the contribution of each of these two different mechanisms. RNA sequencing data supported several of these functional findings. Adhesion and motility regulators such as ITGB5 and SLC3A2 were upregulated, consistent with altered wound closure. Downregulation of EMT pathways aligns with reduced TEER in MDCK cells, reflecting impaired epithelial plasticity and barrier function. Cytoskeletal regulators, including ARHGAP22 and CCND1, were differentially expressed, in line with phalloidin staining that revealed DHA-induced stress fiber remodeling. Together, these transcriptional changes suggest that DHA alters adhesion, cytoskeleton, and junctional integrity, contributing to the observed phenotypes.

Fig. 6 Concentration-dependent changes in hallmark gene set enrichment scores in 2,8-dihydroxyadenine (DHA-treated) HK-2 cells **a**. Heatmap of hallmark gene set enrichment scores across DHA concentrations. Red indicates positive enrichment and blue indicates negative enrichment. **b**. Representative enrichment plots of positively enriched pathways in HK-2 cells treated with 240 µg/mL DHA, including mTORC1 signaling, TNF-α signaling via NF-κB, and PI3K–AKT–mTOR signaling. **c**. Representative enrichment plots of negatively enriched pathways in cells treated with 240 µg/mL DHA, including DNA repair, epithelial–mesenchymal transition, and oxidative phosphorylation. NES = normalized enrichment score ▶


a
HALLMARK_E2F_TARGETS
HALLMARK_G2M_CHECKPOINT
HALLMARK_MITOTIC_SPINDLE
HALLMARK_MTORC1_SIGNALING
HALLMARK_MYC_TARGETS_V1
HALLMARK_MYC_TARGETS_V2
HALLMARK_TNFA_SIGNALING_VIA_NFKB
HALLMARK_UNFOLDED_PROTEIN_RESPONSE
HALLMARK_GLYCOLYSIS
HALLMARK_IL2_STAT5_SIGNALING
HALLMARK_UV_RESPONSE_UP
HALLMARK_PI3K_AKT_MTOR_SIGNALING
HALLMARK_PANCREAS_BETA_CELLS
HALLMARK_UV_RESPONSE_DN
HALLMARK_COMPLEMENT
HALLMARK_DNA_REPAIR
HALLMARK_MYOGENESIS
HALLMARK_PROTEIN_SECRETION
HALLMARK_XENOBIOTIC_METABOLISM
HALLMARK_PEROXISOME
HALLMARK_BILE_ACID_METABOLISM
HALLMARK_HEME_METABOLISM
HALLMARK_FATTY_ACID_METABOLISM
HALLMARK_COAGULATION
HALLMARK_ADIPOGENESIS
HALLMARK_EPITHELIAL_MESENCHYMAL_TRANSITION
HALLMARK_OXIDATIVE_PHOSPHORYLATION
6
4
2
0
-2
-4
60DHA
120DHA
240DHA


b
Enrichment plot: HALLMARK_MTORC1_SIGNALING
Enrichment plot: HALLMARK_TNFA_SIGNALING_VIA_NFKB
Enrichment plot: HALLMARK_PI3K_AKT_MTOR_SIGNALING
Enrichment score (ES)
Ranked list metric (PreRanked)
Rank in Ordered Dataset
Enrichment profile
Hits
Ranking metric scores


c
Enrichment plot: HALLMARK_DNA_REPAIR
Enrichment plot: HALLMARK_EPITHELIAL_MESENCHYMAL_TRANSITION
Enrichment plot: HALLMARK_OXIDATIVE_PHOSPHORYLATION
Enrichment score (ES)
Ranked list metric (PreRanked)
Rank in Ordered Dataset
Enrichment profile
Hits
Ranking metric scores



Previous work supports these results, for example a study by Yan et al. who demonstrated that COM-treated macrophage exosomes reduce HK-2 viability, consistent with our DHA-induced cellular effects. Furthermore, DHA crystal deposition was shown to activate mTOR signaling, oxidative stress, and fibrosis in rodents [26, 27]. CD44 upregulation, as observed in our study, has been implicated in COM adhesion to renal epithelium [11] and fibrotic remodeling

◂**Fig. 7** Summary of overlapping differentially expressed genes and their functional enrichment across three 2,8-dihydroxyadenine (DHA) concentrations in HK-2 cells. a. Venn diagram of 141 genes commonly upregulated across 60, 120, and 240 µg/mL 2,8-dihydroxyadenine. b. Heatmap of the top 10 commonly upregulated genes (log2 fold change, Z-score). c. Venn diagram of 243 genes commonly downregulated across DHA concentrations. d. Heatmap of the top 10 commonly downregulated genes (log2 fold change, Z-score). e. Gene ontology (GO) biological process enrichment of the commonly upregulated genes. f. GO biological process enrichment of the commonly downregulated genes. In e. and f., the x-axis indicates the gene ratio (proportion of genes in each GO term), the y-axis shows enriched GO terms, dot size reflects the number of genes, and dot color represents statistical significance (-log10 false discovery rate [FDR])

[28, 29]. In mouse models of DHA crystal nephropathy, deletion of Tnfr1 reduced tubular CD44 and inflammation, while Tnfr2, Cd44, or Ahsg deletion had little effect [7]. The TEER drop in MDCK cells mirrors findings from COM models where tight junction proteins such as occludin and ZO-1 were reduced [9].

DHA showed dose-dependent effects on gene expression in HK-2 cells through distinct transcriptional profiles at increasing DHA concentrations. Upregulated pathways, including E2F targets, G2M checkpoint, and TNFA signaling, suggest activation of stress response mechanisms, cell cycle dysregulation and inflammatory signaling. These processes are associated with cellular stress, apoptosis, or maladaptive proliferation, consistent with reduced cell viability [30]. The downregulation of EMT and oxidative phosphorylation indicates metabolic alterations and suppression of cellular plasticity, as has been previously shown to occur in cancer stem cells [31]. These results suggest interaction between adaptive responses and metabolic stress at higher DHA concentrations. The activation of mTORC1 and TNF-α signaling indicates an inflammatory state, reflecting cellular adaptation to stress. Metabolic genes like SLC3A2 and GFPT1 showed increased expression, consistent with adaptive stress responses [32, 33]. Decreased expression of the mitochondrial genes CCDC90B, NDUFB3, and ATP5PO compromises ATP production, leading to oxidative stress [34]. Upregulation of ERK1 and ERK2 signaling cascades affects cell signaling and tissue remodeling, while downregulation of oxidative phosphorylation indicates mitochondrial dysfunction [35]. These findings suggest that gene expression changes in kidney epithelial cells involve multiple pathways regulating cell survival and tissue integrity.

Our study has several notable limitations. We used immortalized kidney cell lines rather than cells derived from patients with APRT deficiency or in vivo models. DHA was added exogenously rather than formed in situ as is the case in rodent models of adenine-induced DHA crystal nephropathy. The wound closure assay reflects multiple processes (cell migration, proliferation, and survival) and does not specifically implicate reduced migration as the mediator of delayed wound closure. RNA sequencing was performed only in HK-2 cells and was not validated functionally in other models. Quantification of actin remodeling in COM-treated cells was curtailed due to limited sample availability. Finally, TEER provides a simplified readout of epithelial barrier integrity and cannot fully capture the complexity of kidney fibrosis. Future studies should validate these pathways in physiologically more relevant systems such as patient-derived organoids, 3D co-cultures, or animal models.

In summary, this study shows that DHA exposure alters cell viability, wound closure, CD44 expression, actin remodeling and epithelial barrier function in kidney cell lines. DHA also induces transcriptional changes consistent with inflammation, cytoskeletal remodeling, and metabolic stress. These findings highlight cellular mechanisms underlying kidney injury in APRT deficiency and may implicate potential novel therapeutic targets.

Supplementary Information The online version contains supplementary material available at https://doi.org/10.1007/s00109-025-02625-x.

Acknowledgements The authors would like to thank Snaevar Sigurdsson (BioMedical Center, School of Health Sciences, University of Iceland) for his assistance in acquiring the gene sequencing data and conducting Kallisto and Sleuth analyses. The authors also thank Snorri Thor Sigurdsson (Faculty of Physical Sciences, School of Engineering and Natural Sciences, University of Iceland) for synthesizing the DHA used in the in vitro studies. Finally, the authors thank Adrian Lopez Garcia de Lomana (BioMedical Center, School of Health Sciences, University of Iceland) for his assistance in formatting and uploading the RNA sequencing data to the GEO database.

Author contribution HRH, TG, RP and VOE conceptualized the study and designed the methodology. HRH conducted the data collection and analysis. TG contributed to the interpretation of the results and the literature review. HRH drafted the manuscript, and TG, RP and VOE provided critical revisions. TG and VOE supervised the project. All authors approved the final manuscript for submission.

Funding This work was funded by the Icelandic Research Fund (grant no. 217707-051) and the Landspitali University Hospital Science Fund.

Data availability The original RNA sequencing data presented in the study were submitted to the Gene Expression Omnibus database (GEO) under accession number GSE29597.

Declarations

Conflict of interest The authors declare no competing interests.

Open Access This article is licensed under a Creative Commons Attribution-NonCommercial-NoDerivatives 4.0 International License, which permits any non-commercial use, sharing, distribution and reproduction in any medium or format, as long as you give appropriate credit to the original author(s) and the source, provide a link to the Creative Commons licence, and indicate if you modified the licensed material. You do not have permission under this licence to share adapted material derived from this article or parts of it. The images or other third party material in this article are included in the article's Creative Commons

licence, unless indicated otherwise in a credit line to the material. If material is not included in the article's Creative Commons licence and your intended use is not permitted by statutory regulation or exceeds the permitted use, you will need to obtain permission directly from the copyright holder. To view a copy of this licence, visit http://creativecommons.org/licenses/by-nc-nd/4.0/.

References

1. Runolfsdottir HL et al (2016) Kidney disease in adenine phosphoribosyltransferase deficiency. Am J Kidney Dis 67(3):431–8
2. Edvardsson VO et al (2013) Hereditary causes of kidney stones and chronic kidney disease. Pediatr Nephrol 28(10):1923–1942
3. Edvardsson V et al (2001) Clinical features and genotype of adenine phosphoribosyltransferase deficiency in Iceland. Am J Kidney Dis 38(3):473–80
4. Knauf F et al (2013) NALP3-mediated inflammation is a principal cause of progressive renal failure in oxalate nephropathy. Kidney Int 84(5):895–901
5. Mulay SR et al (2013) Calcium oxalate crystals induce renal inflammation by NLRP3-mediated IL-1beta secretion. J Clin Invest 123(1):236–246
6. Ludwig-Portugall I et al (2016) An NLRP3-specific inflammasome inhibitor attenuates crystal-induced kidney fibrosis in mice. Kidney Int 90(3):525–39
7. Klinkhammer BM et al (2020) Cellular and molecular mechanisms of kidney injury in 2,8-dihydroxyadenine nephropathy. J Am Soc Nephrol 31(4):799–816
8. Shah A, SW Leslie, Ramakrishnan S, Hyperoxaluria, in StatPearls. 2025, StatPearls Publishing
9. Peerapen P, Thongboonkerd V (2011) Effects of calcium oxalate monohydrate crystals on expression and function of tight junction of renal tubular epithelial cells. Lab Invest 91(1):97–105
10. Yu L et al (2017) Calcium oxalate crystals induces tight junction disruption in distal renal tubular epithelial cells by activating ROS/Akt/p38 MAPK signaling pathway. Ren Fail 39(1):440–451
11. Asselman M et al (2003) Calcium oxalate crystal adherence to hyaluronan-, osteopontin-, and CD44-expressing injured/regenerating tubular epithelial cells in rat kidneys. J Am Soc Nephrol 14(12):3155–66
12. Wang B et al (2020) MiRNA-34a inhibits cell adhesion by targeting CD44 in human renal epithelial cells: implications for renal stone disease. Urolithiasis 48(2):109–116
13. Koul S et al (2012) Genome-wide analysis of differentially expressed genes in HK-2 cells, a line of human kidney epithelial cells in response to oxalate. PLoS One 7(9):e43886
14. Zhang L et al (2022) The expression of apoptosis related genes in HK-2 cells overexpressing PPM1K was determined by RNA-seq analysis. Front Genet 13:1004610
15. Pimentel H et al (2017) Differential analysis of RNA-seq incorporating quantification uncertainty. Nat Methods 14(7):687–690
16. Subramanian A et al (2005) Gene set enrichment analysis: a knowledge-based approach for interpreting genome-wide expression profiles. Proc Natl Acad Sci U S A 102(43):15545–15550
17. Liberzon A et al (2015) The molecular signatures database (MSigDB) hallmark gene set collection. Cell Syst 1(6):417–425
18. Omeir RL et al (2011) Heterogeneity of the tumorigenic phenotype expressed by Madin-Darby canine kidney cells. Comp Med 61(3):243–250
19. Ryan MJ et al (1994) HK-2: an immortalized proximal tubule epithelial cell line from normal adult human kidney. Kidney Int 45(1):48–57
20. Graham FL et al (1977) Characteristics of a human cell line transformed by DNA from human adenovirus type 5. J Gen Virol 36(1):59–72
21. Runolfsdottir HL et al (2019) Urinary 2,8-dihydroxyadenine excretion in patients with adenine phosphoribosyltransferase deficiency, carriers and healthy control subjects. Mol Genet Metab 128(1–2):144–150
22. Peerapen P, Thongboonkerd V (2021) Calcium oxalate monohydrate crystal disrupts tight junction via F-actin reorganization. Chem Biol Interact 345:109557
23. Guo L et al (2014) Role of Angptl4 in vascular permeability and inflammation. Inflamm Res 63(1):13–22
24. Srivastava SP et al (2024) Renal Angptl4 is a key fibrogenic molecule in progressive diabetic kidney disease. Sci Adv 10(49):eadn6068
25. Jomova K et al (2023) Reactive oxygen species, toxicity, oxidative stress, and antioxidants: chronic diseases and aging. Arch Toxicol 97(10):2499–2574
26. Moellmann J et al (2024) 2,8-dihydroxyadenine-induced nephropathy causes hexosylceramide accumulation with increased mTOR signaling, reduced levels of protective SirT3 expression and impaired renal mitochondrial function. Biochimica et Biophysica Acta (BBA) 1870(1):166825
27. Yan L, Chen J, Fang W (2022) Exosomes derived from calcium oxalate-treated macrophages promote apoptosis of HK-2 cells by promoting autophagy. Bioengineered 13(2):2442–2450
28. Verhulst A et al (2003) Crystal retention capacity of cells in the human nephron: involvement of CD44 and its ligands hyaluronic acid and osteopontin in the transition of a crystal binding- into a nonadherent epithelium. Am Soc Nephrol 13:107–115
29. Tsuneki M, Madri JA (2014) CD44 regulation of endothelial cell proliferation and apoptosis via modulation of CD31 and VE-cadherin expression. J Biol Chem 289(9):5357–5370
30. Loftus LV, Amend SR, Pienta KJ (2022) Interplay between cell death and cell proliferation reveals new strategies for cancer therapy. Int J Mol Sci 23(9):4723
31. Farahzadi R et al (2023) Oxidative stress regulation and related metabolic pathways in epithelial–mesenchymal transition of breast cancer stem cells. Stem Cell Res Ther 14(1):342
32. Prager GW et al (2007) CD98hc (SLC3A2) interaction with the integrin beta subunit cytoplasmic domain mediates adhesive signaling. J Biol Chem 282(33):24477–84
33. Elbein SC et al (2004) Molecular screening of the human glutamine–fructose-6-phosphate amidotransferase 1 (GFPT1) gene and association studies with diabetes and diabetic nephropathy. Mol Genet Metab 82(4):321–328
34. Kang J et al (2021) Ribosomal proteins and human diseases: molecular mechanisms and targeted therapy. Signal Transduct Target Ther 6(1):323
35. Nowak Gy (2002) Protein kinase C-α and ERK1/2 mediate mitochondrial dysfunction, decreases in active Na+ transport, and cisplatin-induced apoptosis in renal cells*. J Biol Chem 277(45):43377–43388

Publisher's Note Springer Nature remains neutral with regard to jurisdictional claims in published maps and institutional affiliations.